Regularized Gauss-Newton method of nonlinear geophysical inversion in the data space: applications to 3D magnetotelluric inversion

Alexander Gribenko and Michael S. Zhdanov, University of Utah, TechnoImaging, and MIPT*

SUMMARY

One of the most widely used inversion methods in geophysics is a Gauss-Newton algorithm. However, storage and inversion of the Hessian matrix in the model space is computationally expensive. At the same time, the size of the Hessian matrix in the data space can be managed on a workstation for a typical geophysical inverse problem. We have derived a regularized Gauss-Newton (RGN) algorithm in the data space and applied it to a magnetotelluric inverse problem. RGN inversion method was also compared with the preconditioned regularized conjugate gradient (RCG) algorithm. The results of the RGN inversion of MT data collected in the Pavant Butte hydrothermal area indicate that MT sounding represents a valuable method in hydrothermal exploration.

INTRODUCTION

The Gauss-Newton method is one of the most popular approaches to solving inverse problems in geophysics. The major obstacle to applying the Gauss-Newton method in model space is the need to invert a square Hessian matrix with both dimensions equal to the number of model parameters. In modern applications, the number of model parameters can be on the order of millions. Storage and operations with a matrix of this size can be unmanageable on a typical workstation, or even on a moderately sized cluster. Several researchers (Parker, 1994; Siripunvaraporn et al., 2005; Kordy et al., 2016) described and applied Gauss-Newton inversion in the data space. The size of the corresponding square Hessian matrix in the data space is reduced to both dimensions equal to the number of data points. The data space RGN formulation is equivalent to the model space formulation.

We have derived a regularized algorithm of Gauss-Newton inversion in the data space and applied it to the magnetotelluric (MT) inverse problem. A synthetic model study was used to verify our method. The inversion results produced by the Regularized Gauss-Newton (RGN) method in the data space were compared to results of the preconditioned Regularized Conjugate Gradient (RCG) inversion method. The RGN method in the data space provides a robust and reliable inverse problem solution at comparable computational cost. RGN method was applied to the MT data collected in an area with known geothermal resources. The conductivity model recovered by our inversion represents the geological features of the area reasonably well.

TIKHONOV REGULARIZATION

In our formulation we follow the standard Tikhonov regularization procedure (Tikhonov and Arsenin, 1977; Zhdanov, 2002) of minimizing the following parametric functional:

$$P^{\alpha}(\mathbf{m}) = \|\mathbf{r}(\mathbf{m})\|_2^2 + \alpha S(\mathbf{m}), \tag{1}$$

where $\|...\|_2$ is the L_2 norm; $\mathbf{r}$ is the weighted residual difference between predicted and observed data,

$$\mathbf{r}(\mathbf{m}) = \mathbf{W}_d(\mathbf{A}(\mathbf{m}) - \mathbf{d}); \tag{2}$$

$\mathbf{W}_d$ is the matrix of the data weights, often selected as the inverse of the data variance; and $\mathbf{A}$ is the forward modeling operator, applied to the vector of model parameters, $\mathbf{m}$, comprised of the logarithms of conductivity of the individual discretization cells. In the case of magnetotelluric (MT) inversion, forward modeling is based on the contraction integral equations (CIE) method (Hohmann, 1975; Hursán and Zhdanov, 2002; Zhdanov, 2002)) and the MT transfer functions (Cantwell, 1960).

The second term in the parametric functional (1) represents a stabilizer. One of the most common choices of the stabilizing functionals is shown below:

$$S(\mathbf{m}) = \left\|\mathbf{W}_m\left(\mathbf{m} - \mathbf{m}_{apr}\right)\right\|_2^2. \tag{3}$$

Weighting matrix $\mathbf{W}_m$ can incorporate finite difference first derivative matrix, in which case the stabilizer becomes a maximum smoothness (Constable et al., 1987). Model weights based on the integrated sensitivity (Zhdanov, 2002) can also be used in the stabilizer. Finally, regularization parameter α balances the input of the data misfit and stabilization terms of the parametric functional.

REGULARIZED GAUSS-NEWTON METHOD

RGN model update at iteration $k+1$ for the parameter perturbation $\Delta\mathbf{m}_{k+1}$ can be expressed as (Zhdanov, 2002):

$$\Delta\mathbf{m}_{k+1} = -\left(\mathbf{H}^{\alpha}\right)^{-1}\mathbf{l}^{\alpha}(\mathbf{m}_k), \tag{4}$$

where $\mathbf{H}^{\alpha}$ is the matrix of the regularized quasi-Hessian operator:

$$\mathbf{H}^{\alpha} = \mathbf{F}_w^*\mathbf{F}_w + \alpha\mathbf{C}_m. \tag{5}$$

$\mathbf{l}^{\alpha}$ is the regularized direction of the steepest ascent:

$$\mathbf{l}^{\alpha}(\mathbf{m}_k) = \mathbf{F}_w^*\mathbf{r}_w + \alpha\mathbf{C}_m\left(\mathbf{m}_k - \mathbf{m}_{apr}\right), \tag{6}$$

and we use the following notations:

$$\mathbf{F}_w = \mathbf{W}_d\mathbf{F},$$
$$\mathbf{r}_w = \mathbf{W}_d(\mathbf{A}(\mathbf{m}_k) - \mathbf{d}),$$
$$\mathbf{C}_m = \mathbf{W}_m^*\mathbf{W}_m,$$

where $\mathbf{F}$ is a Fréchet derivative (sensitivity) matrix.

The solution (4) can be re-formulated in the "data space", resulting in a much smaller square matrix to be computed and inverted. Indeed, we can rewrite equation (4) as follows:

$$\mathbf{H}^{\alpha}\left(\mathbf{m}_{k+1}-\mathbf{m}_{k}\right)=-\mathbf{l}^{\alpha}\left(\mathbf{m}_{k}\right), \tag{7}$$

equivalently:

$$\left(\mathbf{F}_w^*\mathbf{F}_w+\alpha\mathbf{C}_m\right)\left(\mathbf{m}_{k+1}-\mathbf{m}_{apr}\right)-\left(\mathbf{F}_w^*\mathbf{F}_w+\alpha\mathbf{C}_m\right)\left(\mathbf{m}_{k}-\mathbf{m}_{apr}\right) = -\left[\mathbf{F}_w^*\mathbf{r}_w+\alpha\mathbf{C}_m\left(\mathbf{m}_k-\mathbf{m}_{apr}\right)\right],$$

or:

$$\left(\mathbf{F}_w^*\mathbf{F}_w+\alpha\mathbf{C}_m\right)\left(\mathbf{m}_{k+1}-\mathbf{m}_{apr}\right)=\mathbf{F}_w^*\left[\mathbf{F}_w\left(\mathbf{m}_k-\mathbf{m}_{apr}\right)-\mathbf{r}_w\right]. \tag{8}$$

Solving the last equation with respect to $\mathbf{m}_{k+1}$, we have:

$$\mathbf{m}_{k+1}-\mathbf{m}_{apr}=\left(\mathbf{F}_w^*\mathbf{F}_w+\alpha\mathbf{C}_m\right)^{-1}\mathbf{F}_w^*\left[\mathbf{F}_w\left(\mathbf{m}_k-\mathbf{m}_{apr}\right)-\mathbf{r}_w\right]. \tag{9}$$

Using the following matrix properties, $\left(\mathbf{F}_w^{-*}\right)^{-1}=\mathbf{F}_w^*$ and $(\mathbf{AB})^{-1}=\mathbf{B}^{-1}\mathbf{A}^{-1}$, we modify equation (9) further:

$$\begin{aligned}\mathbf{m}_{k+1}-\mathbf{m}_{apr} &= \\ \mathbf{C}_m^{-1}\left[\mathbf{F}_w^{-*}\left(\mathbf{F}_w^*\mathbf{F}_w\mathbf{C}_\mathbf{m}^{-1}+\alpha\mathbf{I}\right)\right]^{-1}\left(\mathbf{F}_w\left(\mathbf{m_k}-\mathbf{m_{apr}}\right)-\mathbf{r}_w\right) &= \\ \mathbf{C}_m^{-1}\left(\mathbf{F}_w\mathbf{C}_\mathbf{m}^{-1}+\alpha\mathbf{F}_w^{-*}\right)^{-1}\left(\mathbf{F}_w\left(\mathbf{m_k}-\mathbf{m_{apr}}\right)-\mathbf{r}_w\right) &= \\ \mathbf{C}_m^{-1}\mathbf{F}_w^*\left(\mathbf{F}_w\mathbf{C}_\mathbf{m}^{-1}\mathbf{F}_\mathbf{w}^*+\alpha\mathbf{I}\right)^{-1}\left(\mathbf{F}_w\left(\mathbf{m_k}-\mathbf{m_{apr}}\right)-\mathbf{r}_w\right)&.\end{aligned}$$

Finally, we arrive at the following equation for the model update in the data space:

$$\mathbf{m}_{k+1}=\mathbf{C}_m^{-1}\mathbf{F}_w^*\left(\mathbf{H}_d^{\alpha}\right)^{-1}\left(\mathbf{F}_w\left(\mathbf{m_k}-\mathbf{m_{apr}}\right)-\mathbf{r}_w\right)+\mathbf{m}_{apr}. \tag{10}$$

Note that, equation (10) includes inversion of a square matrix of the transformed regularized Hessian, $\mathbf{H}_d^{\alpha}$:

$$\mathbf{H}_d^{\alpha}=\mathbf{F}_w\mathbf{C}_\mathbf{m}^{-1}\mathbf{F}_\mathbf{w}^*+\alpha\mathbf{I}, \tag{11}$$

with both dimensions equal to the number of the data.

Note that, expression (10) involves computing the inverse matrix, $\mathbf{C}_m^{-1}$, of squared model weights. In the case of the maximum smoothness stabilizer weighting matrix $\mathbf{W}_m$ includes a non-diagonal finite difference gradient matrix, inverse of which can be difficult to compute. To avoid this difficulty and still obtain a solution with the properties similar to the maximum smoothness inversion, we assume $\mathbf{W}_m=\mathbf{I}$ and introduce an a priori model, $\mathbf{m}_{apr}$, at iteration $k+1$ as follows:

$$\mathbf{m}_{apr}=(\mathbf{D}+\mathbf{I})\,\mathbf{m}_k, \tag{12}$$

where $\mathbf{D}$ is the finite difference matrix of the first derivatives.

PRECONDITIONED REGULARIZED CONJUGATE GRADIENT METHOD

Another way of avoiding computation of the inverse Hessian matrix (5) in the inverse problem solution is to apply the regularized steepest descent or conjugate-gradient (RCG) methods and their variations (Nocedal and Wright, 1999; Zhdanov, 2002, 2015). These methods are based on the computation of the model updates using the gradient or steepest ascent directions according to formula (6) with further computation of the model update as follows:

$$\mathbf{m}_{k+1}=\mathbf{m}_k-s_k\mathbf{l}_{k+1}^{\alpha}, \tag{13}$$

where s_k is a "step length" computed by a line search method. To improve the convergence rate of a gradient method, one can apply a preconditioning matrix $\mathbf{P}$ (Nocedal and Wright, 1999; Zhdanov, 2002) as follows:

$$\mathbf{h}_{k+1}^{\alpha}=\mathbf{P}^{-1}\mathbf{l}_{k+1}^{\alpha}=\mathbf{P}^{-1}\left(\mathbf{F}_w^*\mathbf{r}_w+\alpha\mathbf{C}_m\left(\mathbf{m_k}-\mathbf{m_{apr}}\right)\right). \tag{14}$$

This expression bears a lot of resemblance to the model update used in the RGN method in the model space, equation (4), with the regularized Hessian matrix, $\mathbf{H}^{\alpha}$, replaced by the preconditioner, $\mathbf{P}$. The idea behind preconditioning is to select an easy to invert matrix $\mathbf{P}$, which best represents the Hessian matrix. A common choice for $\mathbf{P}$ is a diagonal of the Hessian matrix taken to some power:

$$\mathbf{P}=diag\,[\mathbf{H}]^{\gamma}. \tag{15}$$

Different choices of the preconditioner's exponent γ are possible. In our model study, we have computed the conjugate-gradient solutions using variable values of γ to investigate its effect on the inverse problem solution and to compare the results of the preconditioned RCG method to the RGN solution.

MODEL STUDY

We illustrate the inversion methods described above by inversion of the magnetotelluric (MT) data. The MT method is well described in many publications (e.g. Vozoff, 1972; Zhdanov and Keller, 1992; Zhdanov, 2009). Specifics of our magnetotelluric inversion implementation can be found in Gribenko and Zhdanov (2015).

The model used for the synthetic study contained two conductive anomalies of different dimensions and different depths. A regional MT survey was computer simulated with 49 stations arranged in an approximately 60×60 km^2 grid. The top panels of Figures 1 and 2 show the horizontal and vertical sections through the geoelectrical model. The locations of the station are shown by stars in Figure 1. The synthetic observed MT data (full impedance tensor) were computed at 19 frequencies between 0.0001 and 0.1 Hz and contaminated with 3.5% random Gaussian noise.

Figure 1 presents horizontal sections of the true and inverse geoelectrical models. The locations of the sections are indicated by dashed white lines in the top panels of Figure 2. The RCG inversions with three different values of the preconditioner exponent, γ, as well as RGN inversion in the data space were performed. All four inversions converged to an acceptable normalized root mean square error of RMS <1.2. It is apparent from the inversion results that the resolution of the deeper body was improved by increasing the preconditioner exponent γ; however, the shape of the deeper anomaly was slightly distorted. Also, for larger values of γ the inversion produced resistive anomalies not present in the true model in the vicinity of the conductors. The value of the preconditioner exponent, $\gamma = 0.5$, resulted in the fastest convergence rate. The RGN inversion produced a reasonable model as well. The shallow conductor recovered by the RGN inversion appeared less smooth than those obtained by the RCG inversions, possibly due to the work-around used to avoid inversion of the gradient matrix required for a rigorous RGN maximum smoothness inversion in the data space. Figure 2 presents vertical sections

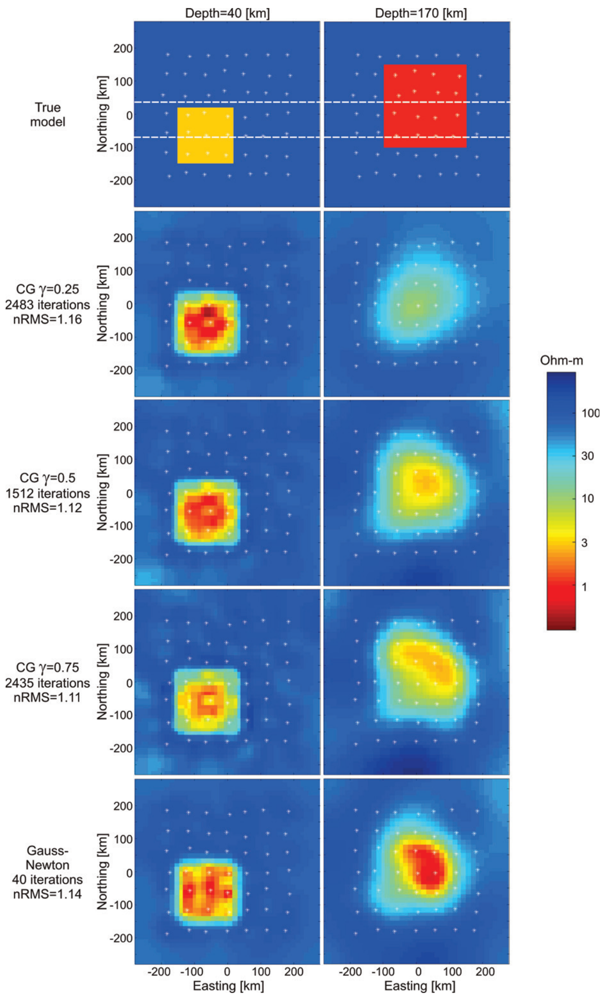

Figure 1: Horizontal sections through the true model (top); second row - RCG inversion with $\gamma = 0.25$; third row - RCG inversion with $\gamma = 0.5$; fourth row - RCG inversion with $\gamma = 0.75$, bottom row - RGN inversion.

of the true and inverse geoelectrical models. The two sections are drawn close to the horizontal centers of the anomalous bodies. The locations of the sections are indicated by the dashed white lines in the top panels of Figure 1. The sections at 40 km appearing in the right panel of Figure 2 show a weak anomaly around the depth of the shallow anomaly due to the proximity of the section to the location of the anomaly. From these vertical sections it can also be noticed that, in the case of the RCG inversion, the resolution of the deeper body was improved with the higher values of the preconditioner exponent, γ. At the same time, the upper body appeared more extended. The resistive anomalies, absent in the true model, were also apparent in the vicinity of the conductors for the higher values of γ. The vertical sections of the RGN inversion result indicate a relatively good resolution of the bottom of the deeper body and of its true conductivity.

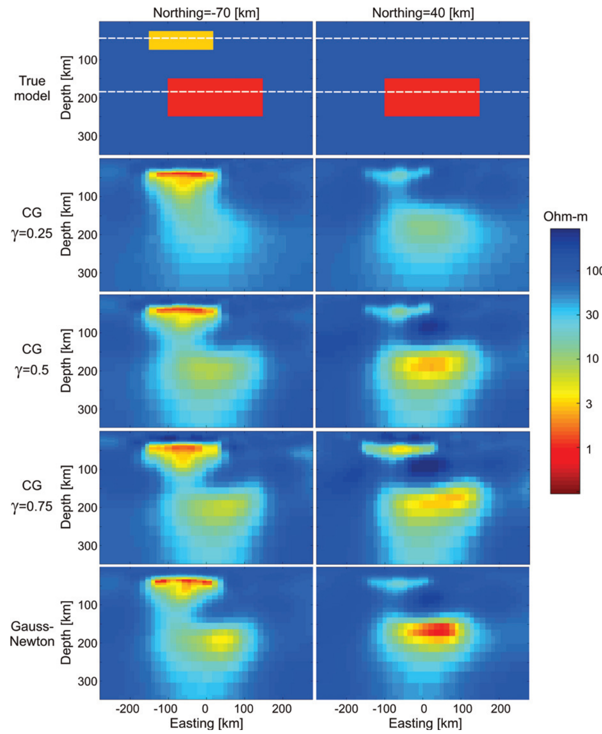

Figure 2: Vertical sections through the true model (top); second row - RCG inversion with $\gamma = 0.25$; third row - RCG inversion with $\gamma = 0.5$; fourth row - RCG inversion with $\gamma = 0.75$; bottom row - RGN inversion.

MT DATA INVERSION AT THE PAVANT BUTTE AREA

In this section, we use MT survey data collected in the Pavant Butte area as an example of the MT field data inversion using the RGN method in the data space. The Pavant Butte area is a part of the Sevier Thermal Belt (Figure 3, panel A). The Sevier Thermal Belt, which represents most of Utah's moderate and high temperature ($>90^oC$) hydrothermal systems, is located in the north-south trending region covering the edge of the Basin and Range province and the Basin and Range-Colorado Plateau transition zone. It is characterized by a high regional heat flow (90 to 150 mWm^{-2}), zones of active seismicity, abundant Late Cenozoic normal faults, Tertiary volcanic and plutonic rocks, and Quaternary basalt and rhyolite. The inversion domain, spreading 94.4 x 56.64 x 32.69 km^3 in the x, y, and z directions, was discretized into rectangular cells of 944 x 944 m^2 in horizontal dimensions with 36 layers ranging from 100 m to 3,162 m in thickness. The full impedance tensor data were used in the inversion. The original data were interpolated on a set of 25 logarithmically spaced frequencies ranging from 0.01 to 100 Hz. Figure 4 shows vertical and horizontal sections of the inversion result. A relatively resistive

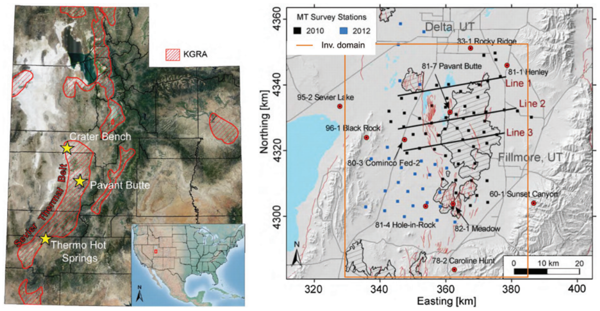

Figure 3: Location map of the survey area. Panel A: the known Geothermal Resource Areas (KGRA) are indicated by the red hatched areas. The Pavant Butte area is indicated by one of the yellow stars. Panel B: a map of the Black Rock Desert and Pavant Butte MT survey area. The orange box outlines approximate horizontal inversion domain boundaries. Adopted from Hardwick (2013).

zone in the central-Northern region at a shallow depth coincides with the surface basalt flows present in the area. This region is highlighted by yellow and light blue colors surrounded by more conductive sediments in the vertical section at 1 km depth. A 3 km horizontal section indicates the presence of the conductive material underlying the basalt flow. The hydrothermal fluids are likely responsible for the areas of elevated conductivity. The source of the hot material is imaged by the conductive body appearing in the western part of the inversion domain. This reservoir is visible in the horizontal section at 12 km depth, as well as in the vertical sections at 4305, 4315, and 4325 km Northing. The multiple pathways of the fluid are imaged, and can be traced in the horizontal sections at 9 and 6 km depths.

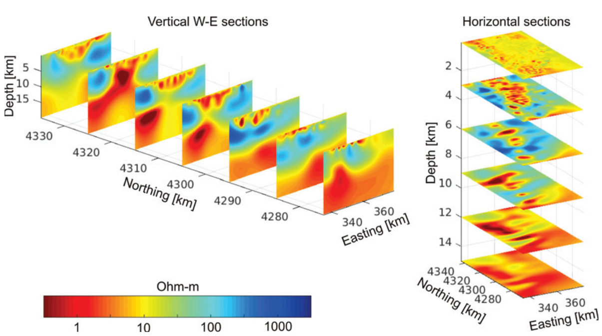

Figure 4: Vertical (left) and horizontal (right) sections of the conductivity distribution obtained by the inversion of the Pavant MT data.

CONCLUSIONS

We implemented the data space regularized Gauss-Newton inversion method in our magnetotelluric inversion. A conventional model space RGN method requires the inversion of the large square Hessian matrix, which is one of the main obstacles for using the RGN method in geophysical inversion. The data space implementation involves inversion of a much smaller matrix, which makes it possible to use the RGN method with limited computer resources. The two formulations are equivalent and yield identical solutions.

We have also outlined a generic regularized conjugate gradient-type method in the model space. The advantage of such methods is that the Hessian matrix and its inversion are not required. However, the RCG method has slower convergence in comparison with the RGN approach. The preconditioners are usually applied to speed up the RCG methods. We have introduced a preconditioner based on the diagonal of the Hessian matrix taken to some power, γ. Our model study has demonstrated that, the different values of preconditioner power, γ, for RCG method can change the resolution of the inverse model at different depths. In our study preconditioner exponent $\gamma = 0.5$ produced better results and faster convergence compared to other RCG solutions. The locations and conductivities of the targets recovered by the RGN method seem to better represent the true model. The artificial resistive anomalies are also absent in the RGN inversion result. Note that, future research will be aimed at improvement of our regularization approach in RGN implementation in order to produce a smoother or sharper inversion result.

We applied our method to MT data collected in the Pavant Butte hydrothermal area. The resistivity distribution recovered by our inversion produced a reasonable representation of the geology of the region. Our study indicates that magnetotelluric sounding represents a useful method in hydrothermal exploration. The inverse conductivity model of the deeper regions may provide valuable information about the geothermal sources.

ACKNOWLEDGEMENTS

We acknowledge the support of the Consortium for Electromagnetic modeling and Inversion (CEMI) at the University of Utah and TechnoImaging. The Pavant Butte MT data were acquired and kindly donated by the Utah Geological Survey for our research.

EDITED REFERENCES

Note: This reference list is a copyedited version of the reference list submitted by the author. Reference lists for the 2017 SEG Technical Program Expanded Abstracts have been copyedited so that references provided with the online metadata for each paper will achieve a high degree of linking to cited sources that appear on the Web.

REFERENCES

Cantwell, T., 1960, Detection and analysis of low frequency magnetotelluric signals: Ph.D. thesis, Massachusetts Institute of Technology.

Constable, S. C., R. L. Parker, and C. G. Constable, 1987, Occam's inversion: A practical algorithm for generating smooth models from electromagnetic sounding data: Geophysics, **52**, 289–300, http://doi.org/10.1190/1.1442303.

Gribenko, A. V., and M. S. Zhdanov, 2015, 3D inversion of regional MT data distorted by near-surface inhomogeneities using a complex distortion matrix: 85th Annual International Meeting, SEG, Expanded Abstracts, 984–989, http://doi.org/10.1190/segam2015-5821800.1.

Hardwick, C., 2013, Geothermal resources in southwestern Utah: Gravity and magnetotelluric investigations: Master's thesis, University of Utah.

Hohmann, G. W., 1975, Three-dimensional induced polarization and electromagnetic modeling: Geophysics, **40**, 309–324, http://doi.org/10.1190/1.1440527.

Hursán, G., and M. S. Zhdanov, 2002, Contraction integral equation method in three-dimensional electromagnetic modeling: Radio Science, **37**, 1–13, http://doi.org/10.1029/2001RS002513.

Kordy, M., P. Wannamaker, V. Maris, E. Cherkaev, and G. Hill, 2016, 3-dimensional magnetotelluric inversion including topography using deformed hexahedral edge finite elements and direct solvers parallelized on symmetric multiprocessor computers — Part II: Direct data-space inverse solution: Geophysical Journal International, **204**, 94–110, http://doi.org/10.1093/gji/ggv411.

Nocedal, J., and S. J. Wright, 1999, Numerical optimization: Springer.

Parker, R. L., 1994, Geophysical inverse theory: Princeton University Press.

Siripunvaraporn, W., G. Egbert, Y. Lenbury, and M. Uyeshima, 2005, Three-dimensional magnetotelluric inversion: Data-space method: Physics of the Earth and Planetary Interiors, **150**, 3–14, http://doi.org/10.1016/j.pepi.2004.08.023.

Tikhonov, A. N., and V. Y. Arsenin, 1977, Solution of ill-posed problems: Winston and Sons.

Vozoff, K., 1972, The magnetotelluric method in the exploration of sedimentary basins: Geophysics, **37**, 98–141, http://doi.org/10.1190/1.1440255.

Zhdanov, M. S., 2002, Geophysical inverse theory and regularization problems: Elsevier.

Zhdanov, M. S., 2009, Geophysical electromagnetic theory and methods: Elsevier.

Zhdanov, M. S., 2015, Inverse theory and applications in geophysics: Elsevier.

Zhdanov, M. S., and G. Keller, 1992, The geoelectrical methods in geophysical exploration: Elsevier.